INTERNATIONAL JOURNAL FOR NUMERICAL METHODS IN ENGINEERING, VOL. 40, 3815–3837 (1997)

IMPROVED VECTOR FEM SOLUTIONS OF MAXWELL'S EQUATIONS USING GRID PRE-CONDITIONING

DANIEL WHITE AND GARRY RODRIGUE*

Department of Applied Science, University of California at Davis and Lawrence Livermore National Laboratory, P.O. Box 808, L-416, Livermore, CA 94551, U.S.A.

ABSTRACT

The Time Domain Vector Finite Element Method is a promising new approach for solving Maxwell's equations on unstructured triangular grids. This method is sensitive to the quality, or condition, of the grid. In this study grid pre-conditioning techniques, such as edge swapping, Laplacian smoothing, and energy minimization, are shown to improve the accuracy of the solution and also reduce the overall computational effort. © 1997 John Wiley & Sons, Ltd.

Int. J. Numer. Meth. Engng., **40**, 3815–3837 (1997)

No. of Figures: 12. No. of Tables: 4. No. of References: 33.

KEY WORDS: Maxwell's equations; wave equation; finite element; vector finite element; Whitney element; grid relaxation

1. INTRODUCTION

Maxwell's equations are a coupled set of linear Partial Differential Equations (PDE's) that describe the time evolution of classical electromagnetic fields. Typically it is desired to solve Maxwell's equations in an inhomogeneous volume consisting of several dielectric, magnetic and metallic regions. Electromagnetic design and analysis problems can be roughly categorized into static problems and dynamic problems. Dynamic problems can again be roughly categorized into those that are best solved in the frequency domain, and those that are best solved directly in the time domain. This study focuses on solution of Maxwell's equations directly in the time domain.

The most popular approach for such problems is the Finite Difference Time Domain method.[1–4] Usually this method is implemented using dual Cartesian grids, with the electric field components known on the primary grid and the magnetic field components known on the dual grid, with the curl operator approximated by the 2nd order central difference formula. The electric field is updated at even time steps, the magnetic field at odd time steps, by 2nd order central difference in time (leapfrog). An alternative method combines the two curl operators and solves the wave equation for either the electric or magnetic field on a single grid. Both approaches yield a conditionally stable and consistent method for solving Maxwell's equations in the time domain. The disadvantage of these finite difference methods is that they are only defined for Cartesian grids, and it has been shown that approximating curved boundaries by a 'stair step'

* Correspondence to: G. Rodrigue, Department of Applied Science, University of California at Davis Hertz Hall, P.O. Box 808, L-416, Livermore, California 94551, U.S.A. E-Mail: white37@llnl.gov, rodrigue@llnl.gov

Contract grant sponsor: United States Department of Energy: Contract grant number: W-7405-Eng-48

CCC 0029–5981/97/203815–23$17.50

Received 8 December 1995
Revised 13 November 1996

approximation can give poor results.[4,5] Nevertheless the FDTD is extremely efficient and it is often used as a benchmark to which new methods are compared.

Whereas FDTD methods are defined on Cartesian grids, Finite Element Methods (FEM) are designed to solve partial differential equations on unstructured grids. Typically curved boundaries are approximated as piecewise linear, and an unstructured mesh is used within each region. The classic FEM using nodal elements has been quite successful in solving static electromagnetic problems where the continuous electrostatic potential can be employed.[6–8] Historically the use of nodal finite elements has been less successful for solving for the electric and/or magnetic fields directly. The use of nodal elements for solving frequency domain Maxwell's equations can lead to spurious modes,[9,10] or numerical solutions that do not satisfy the divergence properties of the fields. Inclusion of divergence conditions into the variational problem can reduce these spurious modes, this is an area of current research.[11] Time domain finite element methods[12,13] may have similar difficulties with spurious modes. If the divergence conditions are neglected, then the divergence of the fields may grow with time, even if the source terms are divergence free. In this case the method does not conserve charge, and is not 'divergence preserving'. In addition nodal finite element methods are not appropriate for inhomogeneous volumes because the electric and magnetic fields are not continuous across a material interface, and it is difficult to correctly model this discontinuity using nodal elements.

Recently developed vector elements, also known as edge elements, Whitney 1-forms, or H(curl) elements,[14–18] have been used to solve Maxwell's equations for the electric and/or magnetic fields directly. These elements have degrees of freedom along the edges of the grid. Since there are in general more edges than nodes, the use of vector finite elements is slightly more expensive than nodal elements for the same grid. However the use of these elements eliminates spurious modes. These elements enforce tangential continuity of the fields but allow for jump discontinuity in the normal component of the fields, which is a requirement for accurate modelling of fields in inhomogeneous volumes. Vector finite element methods have been successfully used in the frequency domain to analyse resonant cavities, compute waveguide modes, and perform scattering calculations.[19–21]

The Time Domain Vector Finite Element Method (TDVFEM), which is derived in Section 2, uses vector finite elements as basis functions in a Galerkin approximation of the vector wave equation. The leapfrog method is used to advance the fields in time. This approach is similar to that developed in Reference 22. It is reasonable to assume that the grid will have some effect on the accuracy of the solution, due to numerical dispersion of the method. The TDVFEM requires that a sparse linear system be solved at every time step. Naturally iterative or approximate methods will be used to solve this system. The computation effort required will depend upon how well conditioned the linear system is, and it is reasonable to assume that this also will depend upon the grid. In this paper a good, or well conditioned, grid will be defined in terms of both numerical dispersion and computational effort required to solve the linear system. The efficacy of pre-conditioning the grid will be examined both analytically and computationally. This study will be limited to two-dimensional grids.

2. THE TIME DOMAIN VECTOR FINITE ELEMENT METHOD

2.1. *Vector wave equation*

In two dimensions, solutions to Maxwell's equations can be decomposed into transverse electric (TE) fields with the electric field in the x, y plane and the magnetic field aligned in the

z direction, and transverse magnetic fields with the magnetic field in the x, y plane and the electric field aligned in the z direction. Both TE and TM fields can be analysed using the TDVFEM, the only difference between the two is the boundary condition. This study was limited to TE fields for simplicity. In this case the two-dimensional Maxwell's equations, (1)–(3), consist of two curl equations that relate the vector electric field $\mathbf{E} = [E_1, E_2]$ and the scalar magnetic field H and a divergence condition.

$$\nabla \times \mathbf{E} = \frac{\partial B}{\partial t} \tag{1}$$

$$\nabla \times H = \frac{\partial}{\partial t} \mathbf{D} \tag{2}$$

$$\nabla \cdot \mathbf{D} = 0 \tag{3}$$

where

$$\nabla \times H = \left[\frac{\partial H}{\partial y}, -\frac{\partial H}{\partial x} \right]^{\mathrm{t}}, \quad \nabla \times \mathbf{E} = \frac{\partial E_2}{\partial x} - \frac{\partial E_1}{\partial y} \tag{4}$$

For simplicity it is assumed there is no current density in the region of interest. Two constitutive relations are required to close Maxwell's equations. For this study the dielectric permittivity ε and the magnetic permeability μ will be considered simple scalar functions of position,

$$\mathbf{D} = \varepsilon \mathbf{E}, \quad B = \mu H \tag{5}$$

The magnetic field is eliminated by applying the operation $\nabla \times$ to equation (1) and applying the identities in equations (2) and (5), we obtain the vector wave equation for the electric field

$$\varepsilon \frac{\partial^2}{\partial t^2} \mathbf{E} = -\nabla \times \frac{1}{\mu} \nabla \times \mathbf{E} \tag{6}$$

2.2. *Vector finite elements*

The Galerkin procedure will be used to solve equation (6) on a two-dimensional triangular grid using linear vector finite elements. More precisely, consider an arbitrary triangle with nodes numbered 1, 2, 3 in a counter clockwise fashion, and let edge $[i, j]$ be the edge connecting nodes i and $j = (i + 1) \bmod 3$. If N_i is the linear nodal basis function associated with node i, then the linear vector finite elements are defined as

$$\mathbf{W}_i = (N_i \nabla N_j - N_j \nabla N_i), \quad j = (i + 1) \bmod 3, \ i = 1, 2, 3 \tag{7}$$

Using the linearity and piecewise smoothness of the nodal basis functions N_i, we readily get the following important properties of the vector elements $\mathbf{W}_i$:

1. $\nabla \cdot \mathbf{W}_i = 0$, i.e. the vector basis functions are divergence free.
2. If $\boldsymbol{\tau}_i$ is the vector from node i to j, then $\boldsymbol{\tau}_i \cdot \mathbf{W}_k(\mathbf{x}_i) = \delta_{ik}$.
3. The tangential components $\boldsymbol{\tau}_i \cdot \mathbf{W}_k$ are continuous across element boundaries while the normal components $\boldsymbol{\tau}_i^{\perp} \cdot \mathbf{W}_k$ are discontinuous.

Property 1 assures that any linear combination of vector finite elements is divergence free within every triangle. Of course the field may be divergent along an edge joining two triangles and is

consistent with a jump in the normal component of the field across a material interface. Property 2 assures the vector finite elements are linearly independent.

Taking the scalar product of both sides of equation (6) with one of the basis functions $\mathbf{W}_j$ and integrating over the domain Ω we get

$$\int_\Omega \varepsilon \frac{\partial^2}{\partial t^2}\mathbf{E}\cdot\mathbf{W}_j\,\mathrm{d}\Omega = -\int_\Omega \nabla\times\frac{1}{\mu}\nabla\times\mathbf{E}\cdot\mathbf{W}_j\,\mathrm{d}\Omega$$

$$= -\int_\Omega \frac{1}{\mu}\nabla\times\mathbf{E}\cdot\nabla\times\mathbf{W}_j\,\mathrm{d}\Omega \tag{8}$$

where the second equality follows from Green's second vector theorem with $\mathbf{n}\times\mathbf{E}=0$ on the domain boundary.

We now assume

$$\mathbf{E} = \sum_i^N \mathbf{W}_i e_i \tag{9}$$

to be a member of $W = \mathrm{span}[W_i]$ where N is the number of internal edges in the grid. Then on substituting equation (9) into equation (8) we get a square system of equations

$$\sum_i \left(\int_\Omega \varepsilon\mathbf{W}_i\cdot\mathbf{W}_j\,\mathrm{d}\Omega\right)\frac{\partial^2 e_i}{\partial t^2} = -\sum_i\left(\int_\Omega \frac{1}{\mu}\nabla\times\mathbf{W}_i\cdot\nabla\times\mathbf{W}_j\,\mathrm{d}\Omega\right)e_i \tag{10}$$

This leads to a system of ordinary differential equations

$$A\frac{\partial^2 e}{\partial t^2} = Ce \tag{11}$$

where e is the N-dimensional vector of Galerkin coefficients. Here,

(1) A is symmetric and positive definite (since $\varepsilon \geqslant 1$);
(2) C is symmetric and negative semidefinite.

In practice it is not necessary to calculate the magnetic field, however we introduce a definition of magnetic field in order to prove stability and conservation of energy. If the magnetic flux density is defined as

$$B = \sum_i b_i T_i, \quad T_i = \begin{cases} 1, & \text{inside triangle } i \\ 0, & \text{otherwise} \end{cases} \tag{12}$$

and then applying equation (1) and the Galerkin procedure we get

$$\sum_i\left(\int_\Omega \mu^{-1}T_i\cdot T_j\,\mathrm{d}\Omega\right)\frac{\mathrm{d}b_i}{\mathrm{d}t} = \sum_i\left(\int_\Omega \mu^{-1}(\nabla\times\mathbf{W}_i)\cdot T_j\,\mathrm{d}\Omega\right)e_i \tag{13}$$

which again leads to a system of ordinary differential equations

$$F\frac{\mathrm{d}b}{\mathrm{d}t} = Ge \tag{14}$$

The matrices in equations (11) and (14) are extremely sparse, in fact each row has at most five non-zero entries, since each edge in the grid interacts with at most four other edges. Matrices with

elements of the form

$$\int_{\Omega} \Phi_i \cdot \Phi_j \, d\Omega \tag{15}$$

are referred to as Gram matrices in the mathematics literature, and mass matrices in the continuum mechanics literature. In our case, the matrices A and F are related to capacitance and inductance, respectively.

3. TIME DIFFERENCING

Equation (11) is integrated in time using second-order central differences to yield the leapfrog scheme which upon rearrangement is

$$e^{n+1} = (2I + \Delta t^2 A^{-1} C) e^n - e^{n-1} \tag{16}$$

Equation (14) is then differenced

$$b^{n+1/2} = b^{n-1/2} + \Delta t \, F^{-1} G e^n \tag{17}$$

This can be written in two-step form as

$$\begin{bmatrix} e^{n+1} \\ b^{n+1/2} \\ e^n \\ b^{n-1/2} \end{bmatrix} = \begin{bmatrix} (2I + \Delta t^2 A^{-1} C) & O & -I & O \\ \Delta t \, F^{-1} G & I & O & O \\ I & O & O & O \\ O & O & \Delta t F^{-1} G & I \end{bmatrix} \begin{bmatrix} e^n \\ b^{n-1/2} \\ e^{n-1} \\ b^{n-3/2} \end{bmatrix} \tag{18}$$

The matrix in equation (18) is called the amplification matrix of the difference method defined by equations (16) and (17).

3.1. *Stability*

The eigenvalues of the amplification matrix are

$$\lambda = \frac{-\tilde{\lambda} \pm \sqrt{\tilde{\lambda}^2 - 4}}{2} \tag{19}$$

where $\tilde{\lambda}$ are the eigenvalues of $2I + \Delta t^2 A^{-1} C$. If Δt satisfies

$$\Delta t \leqslant 2/(\sqrt{\rho(A^{-1} C)}) \tag{20}$$

then because of the fact that the eigenvalues of $A^{-1} C$ are negative we see that the discriminant of equation (19) is negative. It follows that under the condition in equation (20) we have $|\lambda| = 1$ and the method is non-dissipative. A method is dissipative in the sense that if $|\lambda| < 1$ the fields would decrease (dissipate) with increasing time. Consider the time evolution of electromagnetic fields in a closed perfectly conducting cavity. In this case the initial fields simply oscillate in time forever, neither growing nor decreasing in amplitude. If a dissipative time integration method with $|\lambda| < 1$ were used, the fields would decrease in time, which is very non-physical.

Poynting's theorem of energy conservation[23] states that the time rate of change of stored electromagnetic energy in a given volume equals the power supplied to the volume by independent sources, minus the power radiated away from the volume, minus the power dissipated in the volume by conductivity. In a closed cavity without sources to supply power or conductivity to dissipate power, the total energy must remain constant. The total energy in an electromagnetic field is defined as

$$\int_{\Omega} (\varepsilon \mathbf{E} \cdot \mathbf{E} + \mu \mathbf{H} \cdot \mathbf{H}) \, \mathrm{d}\Omega \tag{21}$$

which in our case can also be expressed in terms of the degrees of freedom as

$$(e)^{\mathrm{T}} A e + (b)^{\mathrm{T}} F b \tag{22}$$

However in the TDVFEM the electric and magnetic fields are staggered in time, hence energy is not conserved in the traditional sense. A straight-forward, but tedious, calculation shows that the total energy is conserved in a time-average sense, i.e.

$$(e^{n+1})^{\mathrm{T}} A e^{n+1} + (b^{n+1/2})^{\mathrm{T}} F b^{n+1/2} + (e^{n})^{\mathrm{T}} A e^{n} + (b^{n-1/2})^{\mathrm{T}} F b^{n-1/2} \tag{23}$$

is a constant for all n.

3.2. Dispersion

Let ε and μ be constant and consider free space solutions of equation (6) of the form

$$\mathbf{E} = \mathbf{E}_0 e^{I(\mathbf{k} \cdot \mathbf{x} - \omega t)} \tag{24}$$

where ω, $\mathbf{k} = [k_1, k_2] = k[\cos\theta, \sin\theta]$ are independent of $\mathbf{x}$ and t, and $\mathbf{E}_0$ is independent of t. Then equation (24) is a solution of equation (6) whenever the dispersion relation

$$\omega^2 = c^2 k^2 \tag{25}$$

holds, where $c = 1/(\sqrt{\mu\varepsilon})$. The phase velocity is defined as

$$v = \omega / k \tag{26}$$

which equals the speed of light c. In many media ε and μ are not constant, thus the phase velocity v is not constant. A medium in which the phase velocity of a wave depends upon k is called dispersive. A narrow pulse propagating in such a medium will spread out, or disperse, because each Fourier component of the pulse propagates at a slightly different frequency. A medium in which the phase velocity depends upon the direction of propagation θ is called anisotropic. Some media are both dispersive and anisotropic. As stated in Section 2.1 we are only interested in problems in which ε and μ are constants. However the TDVFEM, like other time domain numerical methods, exhibits numerical dispersion due to the finite grid and the finite time sampling. Thus numerical solutions do not obey equation (25), but rather a much more complicated grid-dependent dispersion relation.

We now determine a numerical dispersion relation that relates ω to $\mathbf{k}$ when implemented on a periodic triangular grid. The grid used for this analysis is obtained by perturbing a grid of equilateral triangles with sides of length Δx by an amount δ in the horizontal direction, see

Figure 1. If we substitute equation (24) into equation (9), we see that

$$e_i(t) = (\mathbf{E}_0 \cdot \boldsymbol{\tau}_i) e^{I(\mathbf{k} \cdot \tilde{x}_i - \omega t)} \tag{27}$$

where $\mathbf{x}_i$ is the midpoint of the edge corresponding to e_i, see Figure 1.

Clearly,

$$e_i^{n+1} - 2e_i^n + e_i^{n-1} = \psi e_i^n, \quad \psi = 2(\cos(\omega \Delta t) - 1).$$

Moreover, if $\boldsymbol{\tau}_i$ is parallel to $\boldsymbol{\tau}_j$, then $e_j(t) = e_i(t) e^{I\mathbf{k} \cdot \Delta \mathbf{x}}$ where $\Delta \mathbf{x} = \mathbf{x}_j - \mathbf{x}_i$ so that equation (16) allows us to write a homogeneous system of equations for $e_1, \ldots, e_6$

$$\left(\psi F - \frac{1}{\mu \varepsilon} \frac{\Delta t^2}{\Delta x^2} G \right) \begin{bmatrix} e_1 \\ e_2 \\ e_3 \\ e_4 \\ e_5 \\ e_6 \end{bmatrix} = 0 \tag{28}$$

where

$$F = \begin{bmatrix} \tilde{A}_{11} & \tilde{A}_{12} & \tilde{A}_{13} & 0 & \tilde{A}_{15} e^{-Ib} & \tilde{A}_{16} e^{-Ib} \\ \tilde{A}_{21} & \tilde{A}_{22} & \tilde{A}_{23}(1 + e^{-Ia}) & \tilde{A}_{24} e^{-Ia} & 0 & 0 \\ \tilde{A}_{31} & \tilde{A}_{32}(1 + e^{Ia}) & \tilde{A}_{33} & \tilde{A}_{34} & 0 & 0 \\ 0 & \tilde{A}_{42} e^{Ia} & \tilde{A}_{43} & \tilde{A}_{44} & \tilde{A}_{45} & \tilde{A}_{46} e^{Ia} \\ \tilde{A}_{51} e^{Ib} & 0 & 0 & \tilde{A}_{54} & \tilde{A}_{55} & \tilde{A}_{56}(1 + e^{Ia}) \\ \tilde{A}_{61} e^{Ib} & 0 & 0 & \tilde{A}_{64} e^{-Ia} & \tilde{A}_{65}(1 + e^{-Ia)} & \tilde{A}_{66} \end{bmatrix}$$

$$G = \begin{bmatrix} \tilde{C}_{11} & \tilde{C}_{12} & \tilde{C}_{13} & 0 & \tilde{C}_{15} e^{-Ib} & \tilde{C}_{16} e^{-Ib} \\ \tilde{C}_{21} & \tilde{C}_{22} & \tilde{C}_{23}(1 + e^{-Ia}) & \tilde{C}_{24} e^{-Ia} & 0 & 0 \\ \tilde{C}_{31} & \tilde{C}_{32}(1 + e^{Ia}) & \tilde{C}_{33} & \tilde{C}_{34} & 0 & 0 \\ 0 & \tilde{C}_{42} e^{Ia} & \tilde{C}_{43} & \tilde{C}_{44} & \tilde{C}_{45} & \tilde{C}_{46} e^{Ia} \\ \tilde{C}_{51} e^{Ib} & 0 & 0 & \tilde{C}_{54} & \tilde{C}_{55} & \tilde{C}_{56}(1 + e^{Ia}) \\ \tilde{C}_{61} e^{Ib} & 0 & 0 & \tilde{C}_{64} e^{-Ia} & \tilde{C}_{65}(1 + e^{-Ia}) & \tilde{C}_{66} \end{bmatrix}$$

and $\tilde{A} = A/\varepsilon \Delta x^2$, $\tilde{C} = \mu C$. That is, equation (27) will be a solution to the difference equation in equation (16) if $\mathbf{e} = [e_1, \ldots, e_6]^t$ is an eigenvector of the symmetric generalized eigenvalue problem $(G - \eta F)\mathbf{e} = 0$.

Using Mathematica (or any other symbolic math package) it is possible to evaluate the six roots η of the equation

$$\det(F - \eta G) = 0 \tag{29}$$

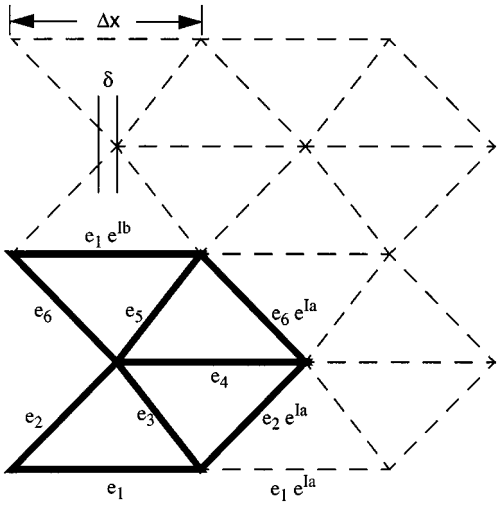

Figure 1. Perturbed grid ($a = k\Delta x \cos\theta$, $b = k\sqrt{3}\,\Delta x \sin\theta$)

as functions of a and b. Although this yields six dispersion relations, only one is consistent in the sense that it approaches the relation in equation (25) as Δt and Δx approach zero. If a Taylor series expansion about $\omega\Delta t = \mathbf{k}\Delta x = 0$ is performed on the consistent dispersion relation, then it can be written as

$$\omega^2\sigma(\omega\Delta t) = c^2k^2\rho_\delta(k\Delta x) \tag{30}$$

where $\sigma(\omega\Delta t)$ represents the isotropic part of the relation and $\rho_\delta(k\Delta x)$ the anisotropic part.

4. EQUILATERAL GRIDS

We now show that certain properties of the TDVFEM are significantly changed when the triangles in a triangular grid are almost equilateral.

4.1. Dispersion

The dispersion relations for $\delta = 0$ corresponding to an equilateral grid are listed in the appendix where we see that the consistent dispersion relation is

$$\sigma(\omega\Delta t) = -1 + \frac{1}{12}(\omega\Delta t)^2 - \frac{1}{360}(\omega\Delta t)^4 + O((\omega\Delta t)^6) \tag{31}$$

$$\rho_{\delta=0}(k\Delta x) = -1 + K_1(k\Delta x)^4 + O((k\Delta x)^6)$$

and

$$K_1 = \frac{7}{11\,520}\sin^6\theta - \frac{1}{768}\sin^4\theta\cos^2\theta + \frac{1}{768}\sin^2\theta\cos^4\theta + \frac{1}{3840}\cos^6\theta$$

Note that the relation is second-order accurate in time and fourth-order accurate in space.

Table I. Anisotropic dispersion coefficients vs. δ

δ	g_1	g_2	g_3	g_4	g_5	g_6	g_7
3/4	− 0·03906	− 0·07031	0·16015	—	—	—	—
1/2	− 0·01736	− 0·03125	0·09722	—	—	—	—
1/4	− 0·00434	− 0·00781	0·02821	—	—	—	—
1/8	− 0·00108	− 0·00195	0·00730	—	—	—	—
1/16	− 0·00027	− 0·00049	0·00194	—	—	—	—
0	0·0	0·0	0·0	− 0·00026	− 0·00061	− 0·00391	0·00130

The numerical dispersion relation was computed for the general case using various perturbations of δ. The general form of the dispersion relation is given by equations (31) and (32). The coefficients for the anisotropic part are listed in Table I.

$$\begin{aligned} \rho_\delta(k\,\Delta x) &= -1 + K_1(k\,\Delta x)^2 + K_3(k\,\Delta x)^4 + O(k\,\Delta x)^6 \\ K_2 &= g_1\cos^4\theta + g_2\sin^4\theta + g_3\cos^2\theta\sin^2\theta \\ K_3 &= g_4\cos^6\theta + g_5\sin^6\theta + g_6\sin^2\theta\cos^4\theta + g_7\sin^4\theta\cos^2\theta \end{aligned} \tag{32}$$

Clearly, the coefficients g_1, g_2, and g_3 in Table I decrease as δ goes to zero. In fact, a simple least-square curve fit indicates that these coefficients are second order in δ indicating that substantial improvement in the computed solution can be gained by conditioning the grid such that the triangular elements are nearly equilateral.

The numerical phase velocity is given by

$$\tilde{v} = \frac{\omega}{k} = c\sqrt{\frac{\rho_\delta(k\,\Delta x)}{\sigma(\omega\,\Delta t)}} \tag{33}$$

Figure 2 shows plots of the numerical anisotropy versus theta, i.e. plots of the numerical phase velocity when $\Delta t = 0$. A value of $\Delta x = \lambda/5$ was used for each plot where $\lambda = 2\pi/k$ is the wavelength. This is generally considered a coarse grid for wave propagation experiments. However, these plots indicate that the numerical anisotropy is quite small even for this grid. The phase velocity error for an equilateral grid is 0·33 per cent. It should be noted that on a Cartesian grid with the same $\Delta x = \lambda/5$, the FDTD algorithm has a phase velocity error of approximately 7·54 per cent. Figure 3 shows the numerical anisotropy versus theta using a grid spacing of $\Delta x = \lambda/10$. This time the equilateral grid has a phase velocity error of 0·0245 per cent.

The fact that the numerical dispersion relation is fourth-order accurate in space for an equilateral grid has been reported by other researchers.[24,25] This result suggests that an equilateral grid should be used for wave propagation experiments where it is desired to keep the numerical anisotropy low. However many electromagnetic design and analysis problems involve complicated boundaries; this was the motivation for an unstructured grid finite element method in the first place. Thus for real problems it may not be possible to use a grid composed entirely of equilateral triangles. The goal of grid preconditioning is to make a grid that conforms to a piecewise linear boundary and is also nearly equilateral. The tables and plots above indicate that a nearly equilateral grid results in a significant improvement in the reduction of numerical anisotropy, thus providing motivation for the application of grid pre-conditioning.

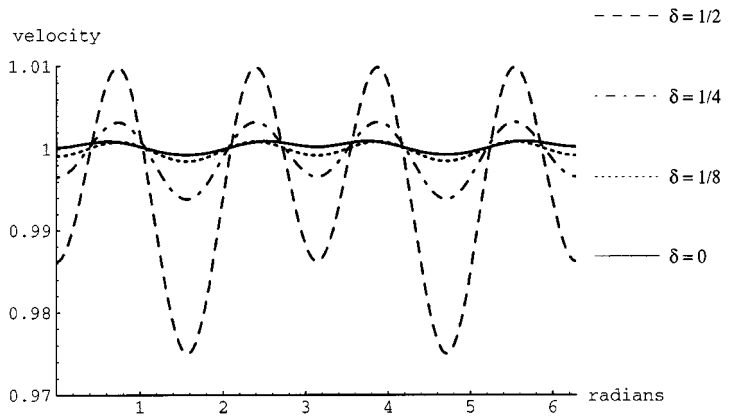

Figure 2. Phase velocity for $\delta = \frac{1}{2}, \frac{1}{4}, \frac{1}{8}, 0$ and $\Delta x = \lambda/5$

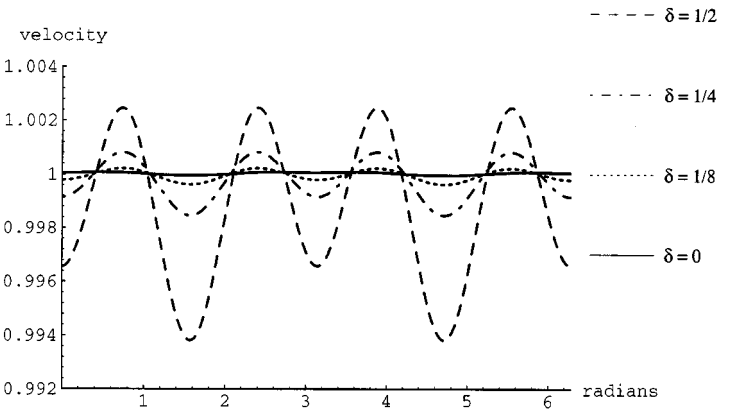

Figure 3. Phase velocity for $\delta = \frac{1}{2}, \frac{1}{4}, \frac{1}{8}, 0$ and $\Delta x = \lambda/10$

4.2. *Diagonal dominance*

The TDVFEM described in equation (16) requires the solution of a linear system $Ax = b$ at every time step. Since the matrix is symmetric and positive-definite, the system can be solved by iterative methods such as fixed point iteration or preconditioned conjugate gradient. In either case, convergence rates of these methods are greatly improved if the matrix A is diagonally dominant. In this section we show that the nearer the grid is to being equilateral, the more diagonally dominant the matrix A becomes.

Consider edge i of a grid with edge angles α and β defined in Figure 4. Row i of matrix A consists of the values $\langle \mathbf{W}_i, \mathbf{W}_i \rangle$, $\langle \mathbf{W}_i, \mathbf{W}_{j_1} \rangle$, $\langle \mathbf{W}_i, \mathbf{W}_{j_2} \rangle$, $\langle \mathbf{W}_i, \mathbf{W}_{j_3} \rangle$ and $\langle \mathbf{W}_i, \mathbf{W}_{j_4} \rangle$, where

$$\langle \mathbf{W}_a, \mathbf{W}_b \rangle = \int_\Omega \mathbf{W}_a \cdot \mathbf{W}_b \, \mathrm{d}\Omega.$$

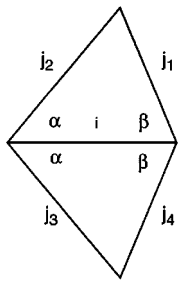

Figure 4. Triangular element with angles α and β

The dominance of row i is defined by the quantity

$$r_i = \frac{\langle \mathbf{W}_i, \mathbf{W}_{j_1} \rangle + \langle \mathbf{W}_i, \mathbf{W}_{j_2} \rangle + \langle \mathbf{W}_i, \mathbf{W}_{j_3} \rangle + \langle \mathbf{W}_i, \mathbf{W}_{j_4} \rangle}{2\langle \mathbf{W}_i, \mathbf{W}_i \rangle} \tag{34}$$

Figure 5 is a plot of r_i versus element angles α and β. The contours are in 0·1 increments. Note that the minimum occurs for the pair $\alpha = \beta = 60^\circ$ which is an equilateral grid. The minimum value in this case is 0·4. For angles $45 < \alpha, \beta < 90$ the matrix A is still very diagonally dominant. There are some combinations of (α, β) such that $r_i > 1$, thus not every grid will yield a diagonally dominant matrix A.

5. GRID PRECONDITIONING

The idea of optimizing a grid to improve the accuracy of a finite element calculation has been studied in the context of structural analysis.[26–28] However the optimal grid for solving Maxwell's equations with the TDVFEM may be quite different than the optimal grid for structural analysis. The previous section provided motivation for using equilateral grids in conjunction with the TDVFEM. There are a variety of commercial and non-profit software packages available for scientists and engineers to use to generate grids. While these grids may be ideal for a variety of different applications, they are not ideal for the TDVFEM in the equilateral sense. Rather than develop a new grid generation method from scratch, we examine different techniques for altering or 'preconditioning' a given grid so as to make it as equilateral as possible while still conforming to a curved boundary.

5.1. Laplace smoothing

Consider a grid of N nodes $V = \{\boldsymbol{v}_1, \boldsymbol{v}_2, \boldsymbol{v}_3, \ldots, \boldsymbol{v}_N\}$ having N_I internal nodes, V_I, and N_B boundary nodes, V_B. Each node $\boldsymbol{v}_i$ is connected to a set of M_i adjacent nodes $C_i = \{\boldsymbol{v}_{i1}, \boldsymbol{v}_{i2}, \ldots, \boldsymbol{v}_{iM_i}\}$. The Laplace matrix of the grid is defined as the $N_I \times N_I$ matrix $L = [l_{ij}]$ where

$$l_{ij} = \begin{cases} M_i, & i = j \\ -1, & \boldsymbol{v}_j \in C_i \cap V_I \end{cases}$$

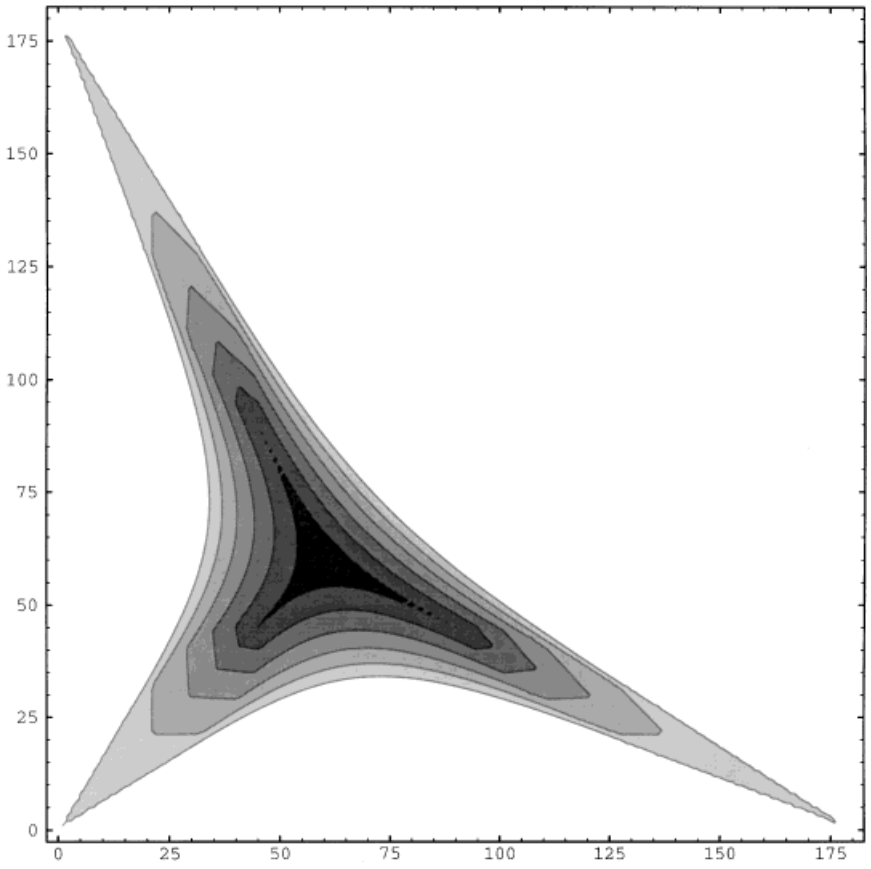

Figure 5. Contour plot of r_i versus element angles (α, β)

A grid is said to be Laplacian smooth if

$$\boldsymbol{v}_k = \left(\sum_{j=1}^{M_k} \boldsymbol{v}_{jk} \right) \Big/ M_k, \quad k = 1, 2, \ldots, N_I \tag{35}$$

or equivalently, the co-ordinates (x_i, y_i) of the nodes satisfy $L\mathbf{x}_I = \mathbf{b}_x$ and $L\mathbf{y}_I = \mathbf{b}_y$, where $\mathbf{x}_I$, $\mathbf{y}_I$ are the vector of internal co-ordinates and $\mathbf{b}_x$, $\mathbf{b}_y$ represent combinations of boundary co-ordinates. Since the matrix L is consistently ordered, symmetric and weakly diagonally dominant, it is non-singular. Consequently, given a set of nodes on the boundary and a connectivity pattern, there exists a unique set of nodes that is Laplace smooth. In this section the boundary nodes and the connectivity pattern is determined by a given computational grid.

Figure 6 illustrates the effect of Laplace smoothing on several triangular discretizations of a circle. Grid 1a consists of a Delaunay triangulation of semi-random points, grid 2a was generated using a divide and conquer approach,[29] and grid 3a was generated using a commercial projection approach.[30] The grids on the right are Laplace smoothed versions of the grids on the left. Figure 7 shows histograms of the edge angles for each of the grids. The vertical axis is the

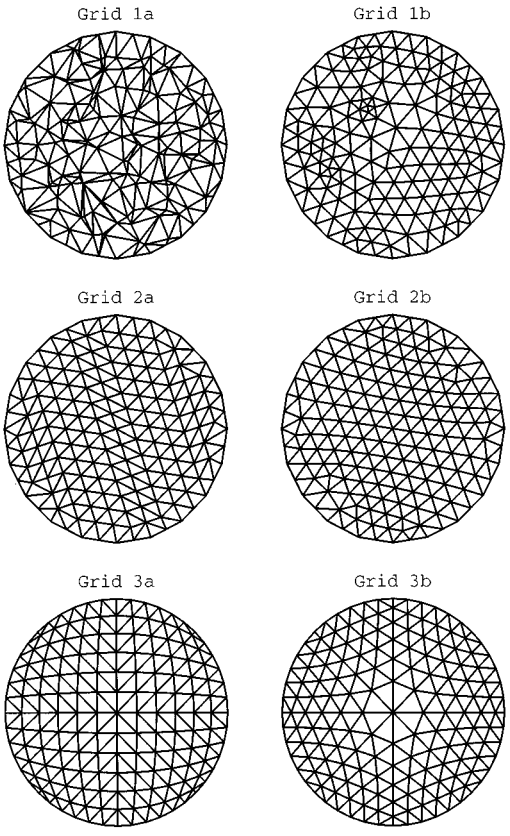

Figure 6. Effect of Laplace smoothing on three different grids

factor of total angles and the horizontal axis is the angle degree divided by 10. The histograms clearly indicate that Laplace smoothing did in fact make the grids closer to equilateral.

5.2. *Edge swapping*

Laplace smoothing tends to make all the angles associated with a node equal, see Figure 7. If a given node is connected to only four nodes, there must be at least one angle $\alpha \geqslant 90$ degrees. Likewise if a given node is connected to eight other nodes, there must be at least one angle $\alpha \leqslant 45^{\circ}$. Consequently, an ideal grid for Laplace smoothing contains internal nodes that are connected to only six other nodes. Since Laplace smoothing does not change the connectivity of the nodes, edge swapping might be employed to improve the connectivity before Laplace smoothing is applied.

Edge swapping was proposed in Reference 31 for the improvement of triangular grids. Consider the example grid shown in Figure 8. The degree of a node is the number of adjacent nodes M_k. Nodes a and b are of degree 7, while nodes c and d are of degree 5. If the edge connecting nodes a and b is 'swapped' to connect nodes c and d, all nodes a, b, c, d will be of degree 6.

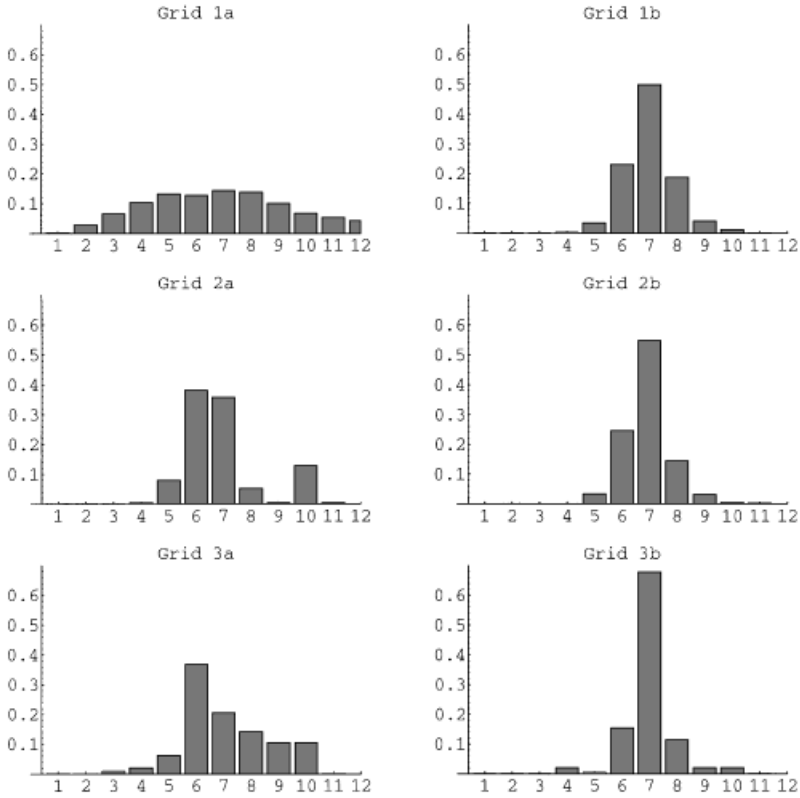

Figure 7. Edge angle histogram demonstrate the effectiveness of Laplace smoothing

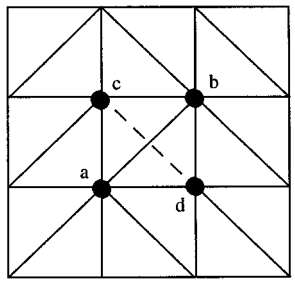

Figure 8. Illustration of edge swapping

The basic algorithm is as follows. The degree of each node is computed, then a swap index is computed for each internal edge in the grid. The swap index for edge i is

$$\text{swap}_i = \deg(a_i) + \deg(b_i) - \deg(c_i) - \deg(d_i) \tag{36}$$

where deg ( ) denotes the degree of the node. If the swap index of the edge is greater than 2 then it is advantageous to swap this edge. The edges with the greatest swap index are swapped first. The

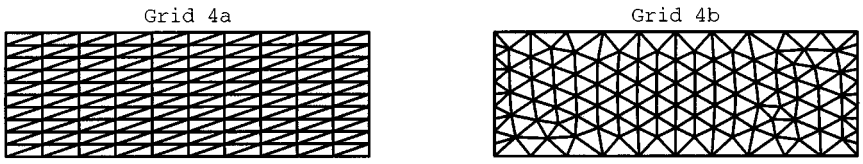

Figure 9. Illustration of grid pre-conditioning via energy minimization for a rectangular cavity

process is repeated until all edges have a swap index of 2 or less. In some situations it is not possible to achieve a swap index of 2 for every edge and an alternative stopping criteria is necessary.[31]

5.3. Grid energy minimization

It is important to note the in some situations neither Laplace smoothing or edge swapping have any effect on the grid. Consider grid 4a in Figure 9 which is a simple triangulation of a Cartesian grid stretched by a factor of three in the x-direction. The internal nodes are already in the centre of their adjacent nodes, thus the equations $L\mathbf{x}_I = \mathbf{b}_x$ and $L\mathbf{y}_I = \mathbf{b}_y$ are already satisfied and the grid is already smooth in the Laplace sense. Also note that each internal nodes are of degree 6, thus there is no benefit to edge swapping. Thus a more radical grid preconditioning approach is required for this type of grid.

Consider defining a grid potential energy function

$$\phi = \sum_{i}^{N} \phi_i, \quad \phi_i = \sum_{j}^{M_i} \left(\frac{\sigma}{r_{ij}} \right)^{12} \tag{37}$$

where N is the number of internal nodes, M_i is the number of nodes adjacent to node i, and r_{ij} is the distance between nodes i and j. The parameter σ is arbitrary constant.

This potential energy function is the repulsive part of the Leonard–Jones potential that is often used in computational molecular dynamics.[32] This is an extremely steep potential function; if the force on node i is defined to be $\mathbf{f}_i = -\nabla\phi_i$ then node i is essentially pushed away from its nearest neighbour. The exponent of 12 in equation (37) is somewhat arbitrary, the idea is for a given node to only feel a force from its immediate neighbours, and not from nodes two or three connections away. Obviously an exponent of only 2 or 3 would not suffice in this regard. Consider grid 4a which is at a local minimum of ϕ since $-\nabla\phi = 0$ and thus there is no net force on any of the nodes. However it is not a global minimum, there are other grids which will have a lower potential energy. Experience indicates that minimum energy grids will be very nearly equilateral. While the absolute global minimum of equation (37) is quite difficult to find, it is possible to perturb the grid and move to the next local minimum by repeatedly moving each node a small amount in the direction of the force. It is essential to re-triangulate the grid after the nodes are moved. Table II lists the grid preconditioning algorithm that is used in the numerical results of the next section.

This algorithm was used to generate grid 4b from grid 4a in Figure 9. The boundary nodes were fixed. The parameters used were $\beta = 0{\cdot}9$, $\sigma = \bar{r}$, $\delta = \bar{r}/10$, where $\bar{r}$ is the initial average distance between adjacent nodes. The algorithm was iterated twenty times. Laplace smoothing was applied as the final step. The resulting grid is significantly better conditioned than the original

Table II. Grid preconditioning algorithm

```
perturb initial grid
re-triangulate
compute initial potential energy φ
compute initial step size δ
begin loop
  compute gradient v = − ∇φ
  compute displacement d = δ(v/(√(v·v)))
  move the nodes x = x + d
  re-triangulate
  swap edges
  compute new φ
  compute new δ = βδ
end loop
Laplace smooth
```

grid, as is demonstrated via computer examples in Section 6. This same procedure was used to generate grid 5b from grid 5a. The initial grid 5a was generated using a divide and conquer approach.[29] This grid represents coaxial cylindrical cylinders, the inner cylinder has a dielectric constant of $\varepsilon = 5$ and the outer cylinder has a dielectric constant of $\varepsilon = 1$. The nodes on the boundary between the two media were constrained.

6. NUMERICAL EXAMPLES

In order to validate the above analyses it is necessary to compare TDVFEM solutions to exact solutions of Maxwell's equations. Consider a two dimensional $1m \times 1/3m$ rectangular cavity with perfectly conducting walls. The electric field vector is confined to the x–y plane and the magnetic field vector is transverse to this plane. This is often referred to as a TE mode. The speed of light is set to unity for convenience. The electric field inside this cavity can be decomposed into an infinite number of modes,

$$\mathbf{E} = \sum_{n,m}^{\infty} \exp(-I\omega_{nm}t)(a_{nm}\hat{x}\cos k_n x \sin k_m y + b_{nm}\hat{y}\sin k_k x \cos k_m y)$$
$$\omega_{nm} = \sqrt{k_n^2 + k_m^2}, \quad k_n = \pi n, \quad k_m = 3\pi m \tag{38}$$

where $\hat{x}$, $\hat{y}$ are the unit vectors in the x and y directions, respectively. The coefficients a_{mn} and b_{nm} depend upon the initial conditions. The TDVFEM can be used to compute the resonant frequencies of a cavity by starting with a random initial electric field and evolving this field in time. The amplitude of the electric field along a selected edge of the grid is stored for every time step. This signal can then be multiplied by a suitable window function and then Fourier transformed to yield the power spectrum. The peaks in the power spectrum are the resonant frequencies of the cavity.

Figure 10 shows the computed power spectrum for grids 4a and 4b. The electric field was updated every 0·017 s for 8000 time steps. The time signal for a selected edge was then multiplied by a Hamming window, and the signal was padded to 16 384 prior to the Fourier transform. As

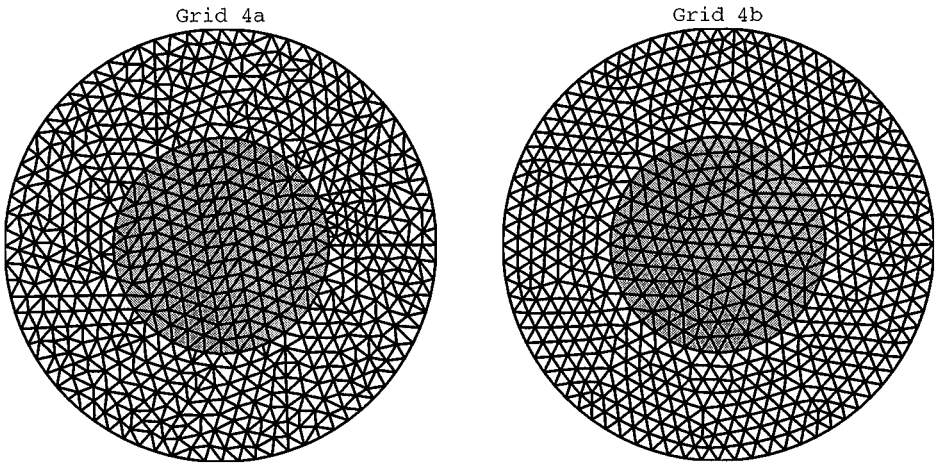

Figure 10. Illustration of grid pre-conditioning via energy minimization for a cylindrical cavity

expected the lower frequencies, which correspond to smaller $\omega \Delta t$ and $k \Delta x$, are more accurate than the higher frequencies.

The same time step and the same Fourier transform process were used for both plots. Note that the computed resonant frequencies for grid 4b are closer to the exact resonant frequencies. There are two modes that resonate at 1·5 Hz, the $n = 3$, $m = 0$ mode and the $n = 0$, $m = 1$ mode. When using grid 4a these two modes oscillate at two different frequencies, one slightly lower than 1·5 Hz and one slightly higher than 1·5 Hz. This is due to the numerical anisotropy of grid 4a. When using grid 4b both modes oscillate at the same frequency. On the interval $0 \leqslant f \leqslant 2$ the rms error was 0·01376 for grid 4a and 0·00333 for grid 4b, thus grid 4b yields a result over four times more accurate than that obtained using grid 4a (Figure 9).

Not only does grid 4b give rise to a more accurate field calculation, it also required less computer time on an HP-750. The conjugate gradient method was used to solve equation (11) to within an error of 10^{-9} at every time step. The calculation on grid 4b required fewer iterations because the resulting matrix A is better conditioned in the sense that it is more diagonally dominant. An even greater reduction in computer time was achieved using adaptive successive over-relaxation. The relaxation parameter was initially set to 1·0 and it was updated at every time step; it quickly converged to an optimal value of 1·07.

The same error criteria of 10^{-9} was used for both the conjugate gradient and the successive over-relaxation methods. The pre-conditioning process required 9·7 s on the HP-750, which is about 9 per cent of the total time required to generate the solution (see Table III).

As a second example consider the coaxial cylinders illustrated in Figure 10. The inner cylinder has a radius of $b = 0{\cdot}5m$ and dielectric constant $\varepsilon_1 = 5{\cdot}0$, the outer has radius $a = 1{\cdot}0m$ and dielectric constant $\varepsilon_2 = 1{\cdot}0$. Using cylindrical co-ordinates the exact solution can be expressed as an infinite number of modes, each mode consisting of Bessel functions of the first and second kind. Each mode oscillates at a resonant frequency. The resonant frequencies are solutions of a complicated transcendental equation that can be solved using a standard root-finding algorithm.

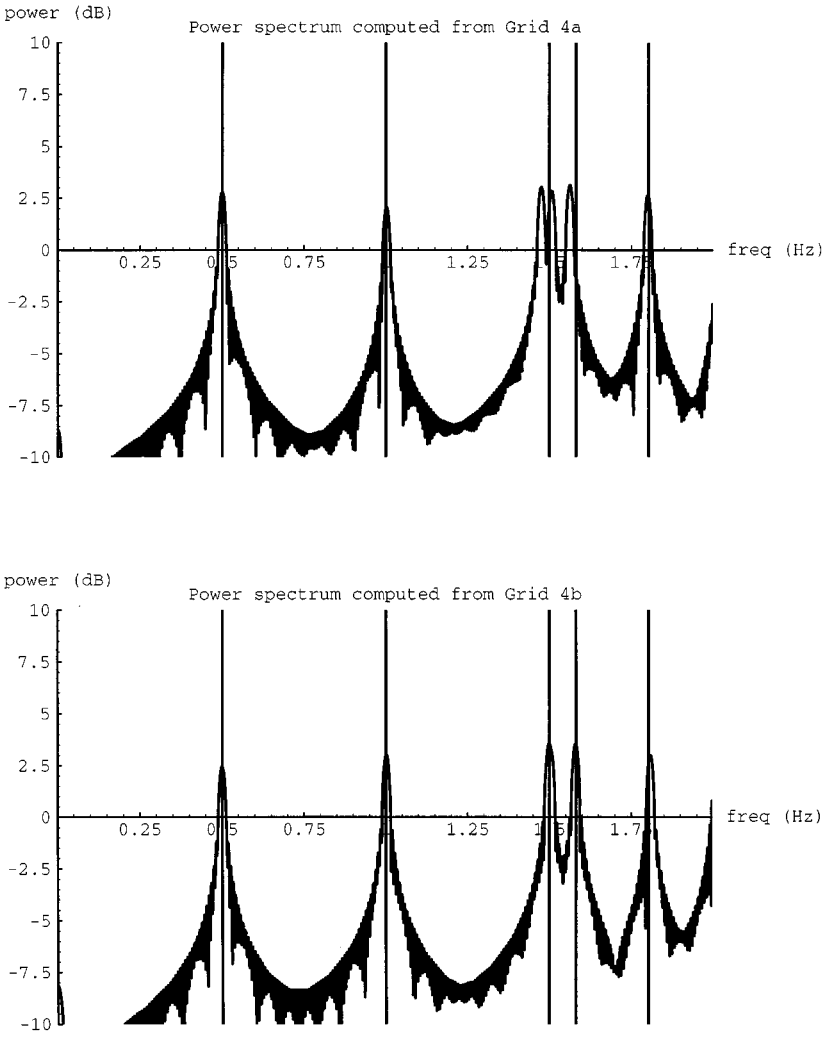

Figure 11. Computed power spectrum using TDVFEM for a $1 \times 1/3$ rectangular cavity

Table III. Computer time required for grids 4a and 4b

Grid	CG	ASOR	Pre-Conditioning
4a	338·2s	210·9s	0
4b	232·5s	110·0s	9·7s

The exact solution is a linear combination of modes

$$E_\rho(n,m) = -I\frac{n}{\varepsilon\rho}(A_{nm}J_n(\rho\omega_{nm}\sqrt{\varepsilon}) + B_{nm}Y_n(\rho\omega_{nm}\sqrt{\varepsilon}))e^{-In\phi}$$
$$E_\phi(n,m) = \frac{\omega_{nm}}{\sqrt{\varepsilon}}(A_{nm}J'_n(\rho\omega_{nm}\sqrt{\varepsilon}) + B_{nm}Y'_n(\rho\omega_{nm}\sqrt{\varepsilon}))e^{-In\phi} \tag{39}$$

where E_ρ and E_ϕ denote the cylindrical components of each mode, J_n and Y_n represent Bessel functions of order n of the first and second kind, and the prime denotes differentiation. The

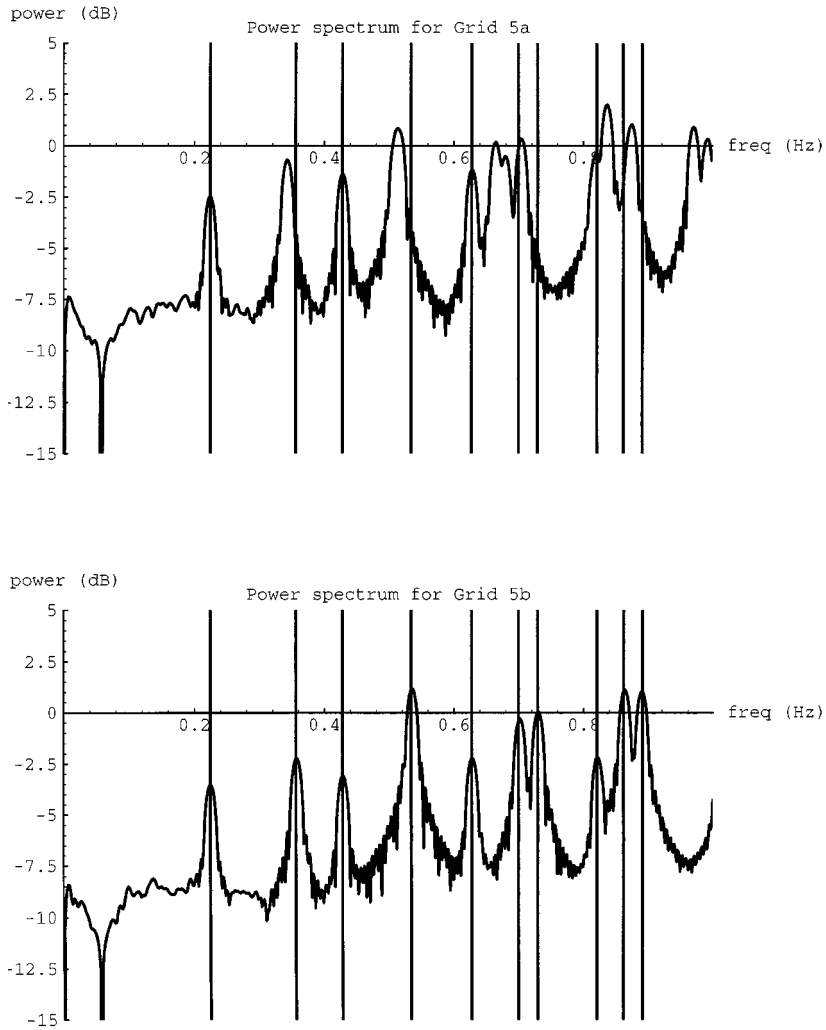

Figure 12. Computed power spectra for coaxial cylindrical cylinder

Table IV. Computer time required for grids 5a and 5b

Grid	CG	ASOR	Pre-conditioning
5a	5488s	1120s	0
5b	4082s	1113s	67s

constants A_{nm} and B_{nm} are given by

$$B_{nm} = \frac{\sqrt{\dfrac{\varepsilon_1}{\varepsilon_2}}\, J'_n(b\omega_{nm}\sqrt{\varepsilon_1})J_n(b\omega_{nm}\sqrt{\varepsilon_2}) - J'_n(b\omega_{nm}\sqrt{\varepsilon_2})J_n(b\omega_{nm}\sqrt{\varepsilon_1})}{J_n(b\omega_{nm}\sqrt{\varepsilon_2})\,Y'_n(b\omega_{nm}\sqrt{\varepsilon_2}) - J'_n(b\omega_{nm}\sqrt{\varepsilon_2})\,Y_n(b\omega_{nm}\sqrt{\varepsilon_2})} \tag{40}$$

$$A_{nm} = \frac{J_n(a\omega_{nm}\sqrt{\varepsilon_1}) - B_{nm}\,Y_n(b\omega_{nm}\sqrt{\varepsilon_2})}{J_n(b\omega_{nm}\sqrt{\varepsilon_2})} \tag{41}$$

The resonant frequency ω_{nm} is the *mth* root of

$$A_{nm}J'_n(a\omega\sqrt{\varepsilon_2}) + B_{nm}\,Y_n(a\omega\sqrt{\varepsilon_2}) = 0 \tag{42}$$

The resonant frequencies for the coaxial cylindrical cylinder were computed using the TDVFEM in the same manner as in the rectangular cavity example. A random initial electric field was generated, the field was updated every 0·017 s for 8000 time steps. The time signal for a selected edge was then multiplied by a Hamming window, and the signal was padded to 16 384 prior to the Fourier transform. The resulting power spectra are shown in Figure 12. The rms error between the computed resonant frequencies and the exact resonant frequencies on the interval $0 \leqslant f \leqslant 1$ was 0·011544 for grid 5a and 0·001259 for grid 5b, thus grid 5b yields a result over nine times more accurate than that obtained using grid 5a. In this example both grids 5a and 5b required comparable computer time. The time required to pre-condition the grid was 67 s, which is about 6 per cent of the total time required to generate the solution (see Table IV).

7. CONCLUSION

Electromagnetic field calculations using the TDVFEM can be improved by various grid pre-conditioning techniques. It was established that an equilateral grid was ideal, but there are advantages towards achieving a nearly equilateral grid. The numerical anisotropy inherent in the TDVFEM is reduced as the grid becomes more equilateral. This was established by an analytical dispersion analysis and verified via two computational experiments. The matrix A, which is similar to the mass matrix in continuum mechanics, becomes very well conditioned as the grid becomes more equilateral. This reduces the computational effort required to update the field. Laplace smoothing consists of moving each internal node to the average of the adjacent nodes; this tends to produce a better conditioned grid in the sense that triangles become more equilateral. Edge swapping can be employed to improve the connectivity of a grid prior to performing Laplace smoothing. In some circumstances a given grid may be smooth in the Laplace sense, but still be rather poorly conditioned. We introduced a new grid pre-conditioning method based on energy minimization principles. This method iteratively moves internal nodes

according to an empirical force law and re-triangulates the grid. Laplace smoothing is then applied as the final step. The resulting grid is much better conditioned than the original.

APPENDIX

The diagonal terms of $\tilde{A}$ are equal to $10/(12\sqrt{3})$, the non-zero off-diagonal terms are all equal to $-1/(12\sqrt{3})$. Every non-zero element $\tilde{C}$ is equal to $4/(\sqrt{3})$. The six solutions to equation (29) are

1.
$$\Psi = 0$$

2.
$$\Psi = 0$$

3.
$$\begin{aligned}\Psi\left(\mu\varepsilon\frac{\Delta\mathbf{x}^2}{\Delta t^2}\right) = & -48 + \frac{4}{3}b^2 + \frac{1}{36}b^4 + \frac{19}{38\,880}b^6 + O(b^7) \\ & + \left(4 - \frac{1}{6}b^2 + \frac{5}{864}b^4 - \frac{127}{933\,120}b^6 + O(b^7)\right)a^2 \\ & + \left(-\frac{1}{4} + \frac{1}{96}b^2 - \frac{23}{41\,472}b^4 + \frac{287}{14\,929\,920}b^6 + O(b^7)\right)a^4 \\ & + \left(\frac{7}{480} - \frac{103}{103\,680}b^2 + \frac{5}{110\,592}b^4 - \frac{11027}{5\,374\,771\,200}b^6 + O(b^7)\right) \\ & \times a^6 + O(a^7)\end{aligned}$$

4.
$$\begin{aligned}\Psi\left(\mu\varepsilon\frac{\Delta\mathbf{x}^2}{\Delta t^2}\right) = & -24 - \frac{9}{4}b^2 + \frac{33}{128}b^4 - \frac{1313}{20\,480}b^6 + O(b^7) \\ & + \left(\frac{9}{4} - \frac{9}{64}b^2 + \frac{471}{4096}b^4 - \frac{8689}{16\,384}b^6 + O(b^7)\right)a^2 \\ & + \left(-\frac{15}{128} - \frac{231}{4096}b^2 + \frac{2867}{65\,536}b^4 - \frac{922583}{31\,457\,280}b^6 + O(b^7)\right)a^4 \\ & + \left(\frac{113}{20\,480} - \frac{1849}{163\,840}b^2 + \frac{467143}{31\,457\,280}b^4 - \frac{101117597}{7\,549\,747\,200}b^6 + O(b^7)\right) \\ & \times a^6 + O(a^7)\end{aligned}$$

5.
$$\begin{aligned}\Psi\left(\mu\varepsilon\frac{\Delta\mathbf{x}^2}{\Delta t^2}\right) = & -\frac{48}{5} + \frac{36}{25}b^2 - \frac{123}{500}b^4 + \frac{1283}{20\,000}b^6 + O(b^7) \\ & + \left(-\frac{36}{25} + \frac{63}{250}b^2 - \frac{2319}{20\,000}b^4 + \frac{42407}{800\,000}b^6 + O(b^7)\right)a^2\end{aligned}$$

$$+\left(-\frac{3}{500}+\frac{1029}{2000}b^2-\frac{70061}{1\,600\,000}b^4+\frac{225263}{7\,680\,000}b^6+O(b^7)\right)a^4$$
$$+\left(\frac{7}{20\,000}+\frac{9287}{800\,000}b^2-\frac{570113}{38\,400\,000}b^4+\frac{12343327}{921\,600\,000}b^6+O(b^7)\right)$$
$$\times a^6+O(a^7)$$

6.

$$\Psi\left(\mu\varepsilon\frac{\Delta x^2}{\Delta t^2}\right)=-\frac{1}{3}b^2+\frac{7}{311\,040}b^6+O(b^7)$$
$$+\left(\frac{1}{768}b^2+\frac{1}{82\,944}b^4-\frac{1}{6\,635\,520}b^6+O(b^7)\right)a^4$$
$$+\left(-1-\frac{1}{6912}b^2-\frac{1}{186\,624}b^6+O(b^7)\right)a^2$$
$$+\left(\frac{1}{3840}+\frac{1}{10\,368}b^2+\frac{47}{19\,906\,560}b^4+\frac{283}{4\,299\,816\,960}b^6+O(b^7)\right)$$
$$\times a^6+O(a^7)$$

Of the six solutions only the last equation makes sense physically.

ACKNOWLEDGEMENT

This research was supported under the auspices of the United States Department of Energy by Lawrence Livermore National Laboratory contract W-7405-Eng-48.

REFERENCES

1. K. S. Yee, 'Numerical solution of initial boundary value problems involving Maxwell's equations in isotropic media', *IEEE Trans. Ant. Prop.*, **14**(3), 302 (1966).
2. A. Taflove and M. E. Brodwin, 'Numerical solution of steady-state electromagnetic scattering problems using the time-dependent Maxwell's equations', *IEEE Trans. Microwave Theory Tech.*, **23,** 623–630 (1975).
3. A. Taflove, 'Review of the formulation and applications of the Finite Difference Time Domain method for numerical modelling of electromagnetic wave interactions with arbitrary structures', *Wave Motion*, **10,** 547–582 (1988).
4. K. S. Kunz and R. J. Luebbers, *The Finite Difference Time Domain Method for Electromagnetics*, CRC Press, Boca Raton, FL, 1993.
5. R. Holland, 'The case against staircasing', *Proc. 6th Annual Review of Progress in Appl. Comput. Electromagnetics*, March 1990, pp. 89–95.
6. O. W. Anderson, 'Laplacian electrostatic field calculations by finite elements with automatic grid generation', *IEEE Trans. Power Apparatus Syst.*, **92**(5), 1485–1492 (1973).
7. P. P. Silvester and R. L. Ferrari, *Finite Elements for Electrical Engineers*, Cambridge University Press, Cambridge, 1983.
8. J. Jin, *The Finite Element Method in Electromagnetics*, Wiley, New York, 1993.
9. A. Bossavit, 'Solving Maxwell equations in a closed cavity, and the question of spurious modes', *IEEE Trans. Magnetics*, **26,** 702–705 (1990).
10. D. Sun, J. Magnes, X. Yuan and Z. Cendes, 'Spurious modes in finite element methods', *IEEE Antenna Propagation Mag.*, **37**(5), 12–24 (1995).
11. B. Jian, J. Wu and L. A. Povinelli, 'The origin of spurious solutions in computational electromagnetics', *J. Comput. Phys.*, **125,** 104–123 (1996).

12. K. Morgan, O. Hassan and J. Peraire, 'An unstructured grid algorithm for the solutions of Maxwell's equations in the time domain', *Int. J. Numer. Meth. Engng*., **19,** 849–863 (1994).
13. J. J. Ambrosiano, S. T. Brandon, R. Lohner and C. R. DeVore, 'Electromagnetics via the Taylor-Galerkin finite element method on unstructured grids', *J. Comput. Phys*., **110,** 310–319 (1994).
14. J. C. Nedelec, 'Mixed finite elements in R3', *Numer. Math*., **35,** 315–341 (1980).
15. A. Bossavit, 'Whitney forms: a class of finite elements for three-dimensional computations in electromagnetism', *IEE Proc*., **135,** pt. A, n. 8, 493–500 (1988).
16. A. Bossavit and I. Mayergoyz, 'Edge elements for scattering problems', *IEEE Trans. Mag*., **25**(4), 2816–2821 (1989).
17. Z. Cendes, 'Vector finite elements for electromagnetic field computation', *IEEE Trans. Mag*., **27**(5), 3948–3966 (1991).
18. J. F. Lee, D. K. Sun and Z. J. Cendes, 'Tangenetial vector finite elements for electromagnetic field computation', *IEEE Trans. Mag*., **27**(8), 4032–4035 (1991).
19. J. Lee, D. Sun and Z. Cendes', 'Full-wave analysis of dielectric waveguides using tangential vector finite elements', *IEEE Trans. Microwave Theory Tech*., **39**(3), 1262–1271 (1991).
20. B. Anderson and Z. Cendes, 'Solution of ferrite loaded waveguide using vector finite elements', *IEEE Trans. Mag*., **31**(3), 1578–1581 (1995).
21. B. Crain and A. Peterson, 'Analysis of propagation on open microstrip lines using mixed-order covariant projection vector finite elements', *Int. J. Microwave Millimeter-Wave CAD*, **5**(20), 59–67 (1995).
22. J. Lee, 'WETD—A finite element time domain approach for solving Maxwell's equations', IEEE Microwave Guided Wave Lett., **4**(1), 11–13 (1994).
23. C. Balanis, *Advanced Engineering Electromagnetics*, Wiley, New York, 1989.
24. P. Monk and A. Parrot, 'A dispersion analysis of finite element methods for Maxwell's equations', *SIAM J. Sci. Comput*., **15**(4), 916–937 (1994).
25. G. Warren and W. Scott, 'Numerical dispersion in the finite elements method using triangular edge elements', *Microwave Opt. Tech., Lett*., **9**(6), 315–319 (1995).
26. M. Pourazday and M. Radhakrishnan, 'Optimization of a triangular mesh', *Comput. Struct*., **40,** 795–804 (1991).
27. R. Martinez and A. Samartin, 'Two-dimensional mesh optimization in the finite element method', *Comput. Struct*., **40,** 1169–1175 (1991).
28. J. H. Cheng, 'Adaptive grid optimization for structural analysis—geometry based approach', *Comp. Meth. Appl. Mech. Eng*., **107,** 1–22 (1993).
29. B. Joe, 'GEOMPACK—A software package for the generation of meshes using geometric algorithms', *Adv. Eng. Software*, **13,** 325–331 (1991).
30. TrueGrid, XYZ Scientific Applications Inc., Livermore CA.
31. W. H. Frey and D. A. Field, 'Mesh relaxation: A new technique for improving traingulations', *Int. J. Numer. Meth. Engng*., **31,** 1121–1133 (1991).
32. W. G. Hoover, *Computational Statistical Mechanics*, Elsevier, New York, 1991.
33. D. A. Field, 'Laplacian smoothing and Delaunay triangulation', *Commun. Appl. Numer. Methods*, **4,** 709–712 (1988).

